Journal of Power Sources 185 (2008) 633–640

Contents lists available at ScienceDirect

Journal of Power Sources

journal homepage: www.elsevier.com/locate/jpowsour

Ni and metal aluminate mixtures for solid oxide fuel cell anode supports

Bu Ho Kwak[a], Hyun Ki Youn[a], Jong Shik Chung[a,b,*]

[a] Department of Chemical Engineering, POSTECH, Pohang 790-784, Republic of Korea
[b] School of Environmental Science and Engineering, POSTECH, Pohang 790-784, Republic of Korea

ARTICLE INFO

Article history:
Received 3 July 2008
Received in revised form 2 September 2008
Accepted 2 September 2008
Available online 16 September 2008

Keywords:
Solid oxide fuel cell
Ni–MAl_2O_4 mixtures
Electrical conductivity
Microstructure

ABSTRACT

Mixtures of nickel and metal aluminate (Ni–$\mathbf{M}Al_2O_4$ [**M** = Fe, Co, Ni and Cu]) were fabricated, and their electrical conductivities, microstructures and thermal expansions were measured. During the sintering of these mixtures, $\mathbf{M}Al_2O_4$ reacts with NiO to form $NiAl_2O_4$ and MO_x which are thought to be the reasons for the differences in the microstructures and electrical properties. Except for $FeAl_2O_4$, Ni–$\mathbf{M}Al_2O_4$ mixtures show metallic conductivity behavior and their electrical conductivities are sufficient for cell operation. Their thermal expansion coefficients are much lower than conventional Ni-YSZ mixtures and closer to the 8YSZ electrolyte. The peak power densities of single cells supported with Ni–$NiAl_2O_4$ and Ni–$CoAl_2O_4$ are 410 and 440 mW cm^{-2} at 850 °C, respectively, which are lower than 490 mW cm^{-2} of Ni-YSZ. This is due to the polarization resistances of functional anode layer. The Ni–$CuAl_2O_4$-supported cell has no electrical performance because of Cu migration and segregation.

1. Introduction

The solid oxide fuel cell (SOFC) is a highly efficient power generating system that can directly use hydrocarbons as a fuel source and can be combined with a gas turbine system [1]. For the fabrication of SOFCs, two different types of supports have been used, namely, electrolyte and anode supports [2], the latter of which is more popular. In anode-supported cells (Fig. 1 left), a thin yttria-stabilized zirconia (YSZ) film is coated on the thick anode support, which is composed of Ni-YSZ cermet [3–5]. Ni-YSZ supports have been used for a long time due to their superior properties, including, high electrical conductivity, high gas permeability, and good catalytic activity. However, Ni-YSZ supports can increase manufacturing cost due to their large volume fraction. Ippommatsu et al. [6] have reported that the manufacturing cost of Ni-YSZ supports is almost 40% of the cost of the planar-type single cell.

Many researches are working on bringing down the costs of raw material and fabrication processes for the commercialization of SOFC. In the anode supports, the electrocatalytic reactions take place in a thin (10–15 μm) area between the electrolyte and the anode interface. The rest of anode support provides for gas transport and an electrical pathway. Therefore, it is possible to make new kinds of single cells coated with thin catalytic layers on the thick electroconducting support (Fig. 1 right). All of the following have been considered as candidates of the SOFC supports: porous metal supports using Fe–Cr alloy or Ni [7–9], Ni cermets based on TiO_2 and Al_2O_3 [10–12], and mixed ionic-electronic conductors (MIEC) [13].

Carbon deposition on the anode, which is caused by the use of hydrocarbon fuels, is another issue that should be resolved in SOFCs. Cokes, which are easily generated on the surface of Ni particles, deactivate the cell performance at high operation temperatures [14]. To avoid this, larger amounts of steam should be supplied along with fuel [15]. Anodes made up of Cu/YSZ composites with CeO_2 [16], Cu/YZT [17], and metal-doped lanthanum chromites [18,19] without Ni doping have been studied for their success in preventing carbon formation. These anodes are stable at low steam/carbon ratio conditions; however, no materials have shown higher catalytic activity or endurance than Ni-based cermets. Ni-doped alumina and Ni-doped metal-aluminate ($NiAl_2O_4$, $CoAl_2O_4$) are well-known hydrocarbon reforming catalysts, which have high mechanical strength and resistance against carbon deposition [20,21]. When porous Ni–$\mathbf{M}Al_2O_4$ (**M** = Fe, Co, Ni, Cu) mixtures are applied as anode supports, they reduce the cost of raw materials and improve the mechanical stability in a direct hydrocarbon SOFC system.

This paper investigates Ni–metal aluminate mixtures that contain various kinds of transition-metals (Fe, Co, Ni and Cu) for possible application as anode supports in SOFC. The physical properties and microstructures of these mixtures are measured and compared in relation to the measured activity of Ni-YSZ anode supports.

* Corresponding author at: Department of Chemical Engineering, POSTECH, San 31, Hyoja-Dong, Nam-Ku, Pohang 790-784, Republic of Korea. Tel.: +82 54 279 2267; fax: +82 54 279 5528.
E-mail address: jsc@postech.ac.kr (J.S. Chung).

0378-7753/$ – see front matter © 2008 Elsevier B.V. All rights reserved.
doi:10.1016/j.jpowsour.2008.09.009

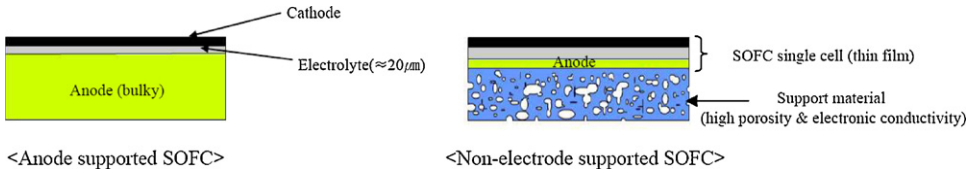

Fig. 1. Comparison between anode-supported and non-electrode-supported SOFC design.

2. Experimental

2.1. Sample preparation

Metal aluminate (MAl_2O_4) powders were prepared by the impregnation method. The metal nitrate hydrates ($Ni(NO_3)_2{\cdot}6H_2O$, $Co(NO_3)_2{\cdot}6H_2O$, $Cu(NO_3)_2{\cdot}xH_2O$ and $Fe(NO_3)_3{\cdot}9H_2O$) were dissolved into distilled water. The dissolved solution was mixed with a stoichiometric amount of Al_2O_3 (AKP-30, Sumitomo Chemical Co.) powder and dried at 100 °C for 3 h. Metal aluminate samples were obtained after calcined at 1200 °C for 5 h. NiO–**M**Al_2O_4 mixtures were prepared by mixing the **M**Al_2O_4 powder and NiO powder (>99%, J.T. Baker) in various ratios to obtain cermets with final NiO contents of 20, 30, 40, 50 and 60 wt%. The mixed powder was ball-milled in an alumina bottle with alumina balls and ethanol for 2 weeks. After drying in an oven, a disk-type support was prepared by uniaxially pressing and sintering in air at 1400 °C for 3 h. This was followed by H_2 reduction in a flow of 5% H_2/He at 850 °C for 5 h to obtain reduced Ni–**M**Al_2O_4. A reference sample of NiO-YSZ cermet was also prepared by mixing 55 wt% NiO with YSZ (TZ-8Y, TOSOH) to make 40 vol% Ni contents after reduction.

2.2. Sample characterization

A bar-type of the support (2 mm × 3 mm × 15 mm) was prepared by cutting the disk-type support in order to measure electrical conductivity. The electrical conductivity was measured by the 4-probe DC technique with Pt wires bending around the bar. The microstructures of reduced NiO–**M**Al_2O_4 mixtures were analyzed by scanning electron microscopy (FE–SEM, Hitachi S4300SE, Japan), and each phase was identified by an energy dispersive X-ray spectrometer (EDX). In order to analyze phase state, the XRD (Cu Kα) measurement and XANES spectra (beamline 3C1 of the Pohang Accelerator Laboratory, POSTECH, Korea) were used. The thermal expansion coefficient of the reduced mixtures was measured by a dilatometer between room temperature and 1000 °C.

2.3. Single cell test

The **M**Al_2O_4 powder that was prepared by impregnation and 50 wt% NiO powder were mixed together to make the cell support. The mixed powder was pressed into 20 mm-diameter disk under 200 MPa, followed by pre-sintering at 1100 °C for 2 h. To make the thin anode layer and electrolyte film, NiO-YSZ (50:50 wt%) powder and YSZ powder were suspended in isopropanol. The suspensions of NiO-YSZ and YSZ were deposited one by one on the disk surface of the Ni–**M**Al_2O_4 support by a spray-coating method. The spray-coated Ni–**M**Al_2O_4 disk was co-fired at 1400 °C for 3 h. LSM–YSZ and pure LSM ($(La_{0.8}Sr_{0.2})_{0.98}MnO_3$, NexTech Materials, Ltd.) powder were used as cathode materials. The cathode powder (90 wt%), polyvinyl butyral (5 wt%) and polyethylene glycol (5 wt%) were mixed together in isopropanol and ball-milled for 12 h to make a slurry. The LSM–YSZ and LSM slurries were coated (0.7 cm × 0.7 cm) one by one on the electrolyte film by stencil printing and fired at 1200 °C for 3 h in air.

Fig. 2 shows the instrument for cell performance measurement. The single cell was attached to the alumina tube and sealed with an zirconia paste (Ultra-Temp 516, Aremco products, Inc.). Platinum meshes were attached to the both sides of the electrodes for current collection, and Pt wire was connected to each platinum mesh. Two small alumina tubes were placed in tight contact with the both electrode sides to reduce the contact resistance. Operation temperature was controlled using a tube furnace, and cell performance was measured with an electronic loader at 850 °C. Fuel, which was in the form of H_2 with 3% H_2O, was fed to the anode side, and air was fed as the oxidant to the cathode side.

3. Results and discussion

3.1. Electrical conductivity and microstructure

The electrical conductivities of the Ni–**M**Al_2O_4 mixtures under reducing conditions (5% H_2 balanced with He) were measured by means of a 4-probe dc method. Fig. 3 shows that electrical

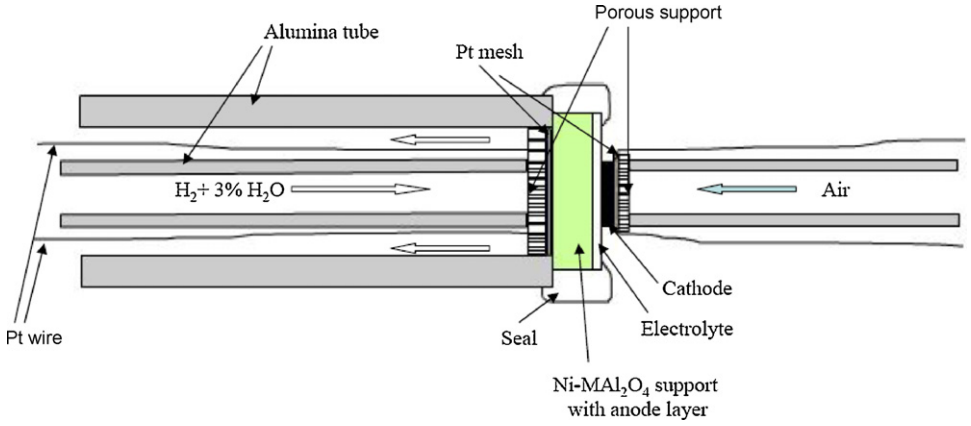

Fig. 2. Configuration of the single cell testing instrument.

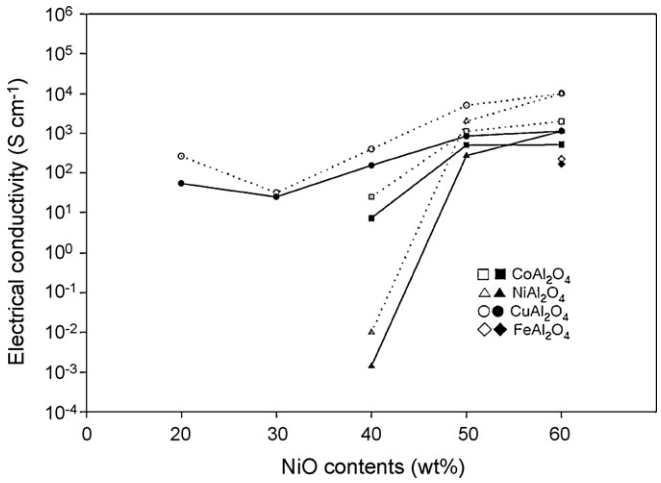

Fig. 3. The electrical conductivities of the Ni–$\mathbf{M}Al_2O_4$ mixture as a function of NiO contents, measured at 20 °C (dotted line), 800 °C (solid line) under H_2 conditions.

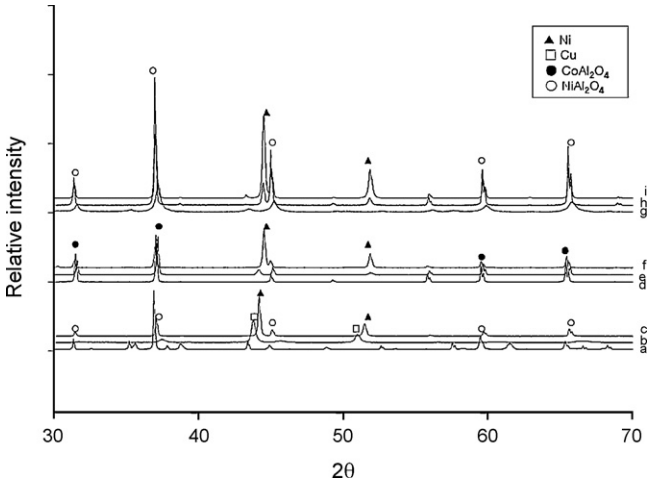

Fig. 5. X-ray diffraction patterns of the reduced Ni–$\mathbf{M}Al_2O_4$ mixtures. (a–c) pure $CuAl_2O_4$, 20 wt%, 50 wt% NiO and (d–f) pure $CoAl_2O_4$, 20 wt%, 50 wt% NiO and (g–i) pure $NiAl_2O_4$, 20 wt%, 50 wt% NiO. $NiAl_2O_4$ and $CoAl_2O_4$ can be distinguished by the three major peaks. The 2θ values of $CoAl_2O_4$ are 31.4, 37.0, and 65.4. $NiAl_2O_4$ are 37.0, 45.0 and 65.6.

conductivities are greatly affected by NiO contents and temperature. In all cases, the conductivities of samples decrease at high temperature (800 °C), which implies that Ni–$\mathbf{M}Al_2O_4$ mixtures have metallic conductivity behavior that comes from the metallic Ni phase. Ni–$CuAl_2O_4$ mixture shows higher electrical conductivity than any other mixtures and sustains good conductivity even at low NiO contents. Ni–$CoAl_2O_4$ and Ni–$NiAl_2O_4$ mixtures show almost same electrical properties, and they exhibit a sudden increase in conductivity above 40 wt% NiO. We believe that the metallic regions of the mixture are disjointed below 40 wt% and that there is no conductance. When NiO content exceeds 40 wt%, continuous conducting networks are formed, and electrical conductivity increases rapidly. This phenomenon is known as the percolation threshold [22]. Ni–$FeAl_2O_4$ samples show no electrical conductivity except for the 60 wt% NiO sample. The reference sample of reduced NiO-YSZ cermet containing 55 wt% NiO shows 6500 S cm^{-1} at room temperature and 1500 S cm^{-1} at 800 °C. These values are close to the conductivity values of Ni–$\mathbf{M}Al_2O_4$ samples except Ni–$FeAl_2O_4$, indicating that Ni–$\mathbf{M}Al_2O_4$ has a conductivity that is sufficient for the operation of SOFC.

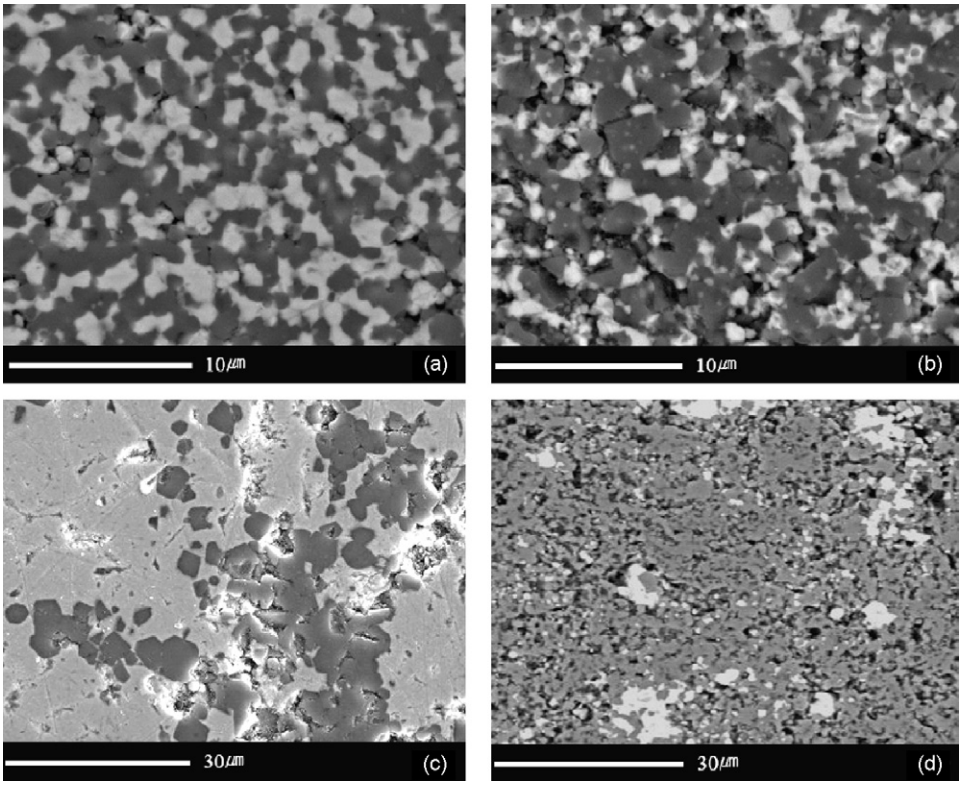

Fig. 4. The microstructures of 50 wt% NiO–$\mathbf{M}Al_2O_4$ mixtures after sintering at 1400 °C and reducing: (a) Ni–$CoAl_2O_4$, (b) Ni–$NiAl_2O_4$, (c) Ni–$CuAl_2O_4$ and (d) Ni–$FeAl_2O_4$. The gray color shows the Ni phase.

It is well known that electrical conductivity is greatly affected by the Ni distribution in the anode cermet [23,24]. To understand the conductivity result, the microstructures of the Ni–$\mathbf{M}Al_2O_4$ mixtures were studied by image analysis. Fig. 4 shows the SEM images of Ni and metal aluminate distributions in the Ni–$\mathbf{M}Al_2O_4$ mixtures. The distribution of the Ni phase seems to be affected by the kinds of metal aluminate powder. In the cases of the Ni–$CoAl_2O_4$ and Ni–$NiAl_2O_4$ mixtures, fine-grained Ni and metal aluminate particles were uniformly distributed (Fig. 4a and b), and this microstructure is very similar to that of the commercial Ni-YSZ cermet [25]. In the case of Ni–$CuAl_2O_4$, the SEM image (Fig. 4c) indicates that the metallic phase covers a large area and metal aluminate particles are isolated in the Ni–$CuAl_2O_4$ mixture. Copper seems to help metallic phase segregation and densification, which offers sufficient electrical contact. The Ni–$FeAl_2O_4$ mixture (Fig. 4d) has only a small amount of Ni phase area, and Ni particles grow to bigger size (≈10 μm), which reduces Ni-to-Ni connection. These microstructures explain why the Ni–$CuAl_2O_4$ mixture has high conductivity but the Ni–$FeAl_2O_4$ mixture has no conductivity.

3.2. Phase analysis

In the previous section, the microstructures of Ni–$\mathbf{M}Al_2O_4$ mixture are changed by the kinds of transition-metals (Fe, Co, Ni and Cu), and these microstructures make a difference in electrical conductivity. To understand the reason for microstructure difference, the phase states of Ni–$\mathbf{M}Al_2O_4$ were checked. Fig. 5 is the XRD patterns of 0, 20, 50 wt% NiO with $\mathbf{M}Al_2O_4$ mixtures after H_2 reduction. The patterns show that $NiAl_2O_4$ crystals are synthesized when NiO ratios are increased. In the case of the Ni–$CuAl_2O_4$ mixtures, $CuAl_2O_4$ crystal peaks (Fig. 5a) disappear when NiO is added (Fig. 5b and c). Reduced 20 wt% NiO–$CuAl_2O_4$ pattern has Cu-peaks with $NiAl_2O_4$. This shows that NiO reacts with alumina when Cu ions escape from metal-aluminate crystals to become Cu metal. EDX results (Fig. 6) also show that Ni ions are exchanged with Cu. Cu metal possesses 80 wt% of metallic phase (spectrum 2) and Ni is dissolved into the metal aluminate structure (spectrum 3). The existence of copper seems to induce the continuous metallic network in the Ni–$CuAl_2O_4$ mixture, even with a small amount of NiO (20 wt%). In XRD patterns, reduced

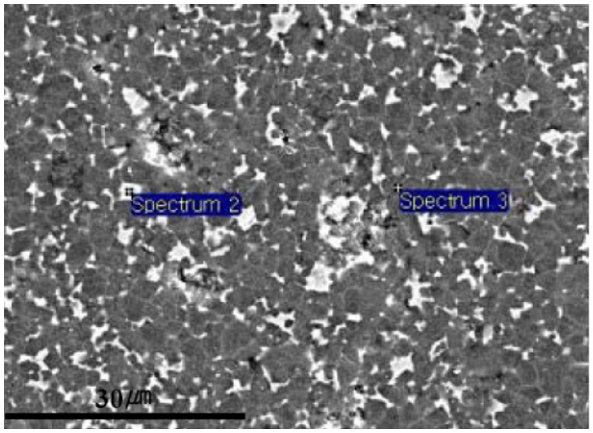

Spectrum 2

Element	Weight%	Atomic%
O	2.67	9.37
Al	2.75	5.72
Ni	16.33	15.64
Cu	78.26	69.26
Totals	100.00	

Spectrum 3

Element	Weight%	Atomic%
O	27.38	47.35
Al	34.51	35.40
Ni	18.24	8.60
Cu	19.87	8.65
Totals	100.00	

Fig. 6. Energy dispersive X-ray spectrometer image of the reduced 20 wt% NiO–$CuAl_2O_4$ mixture, spectra 2 and 3, which shows the elements of metallic phase and metal-aluminate phase.

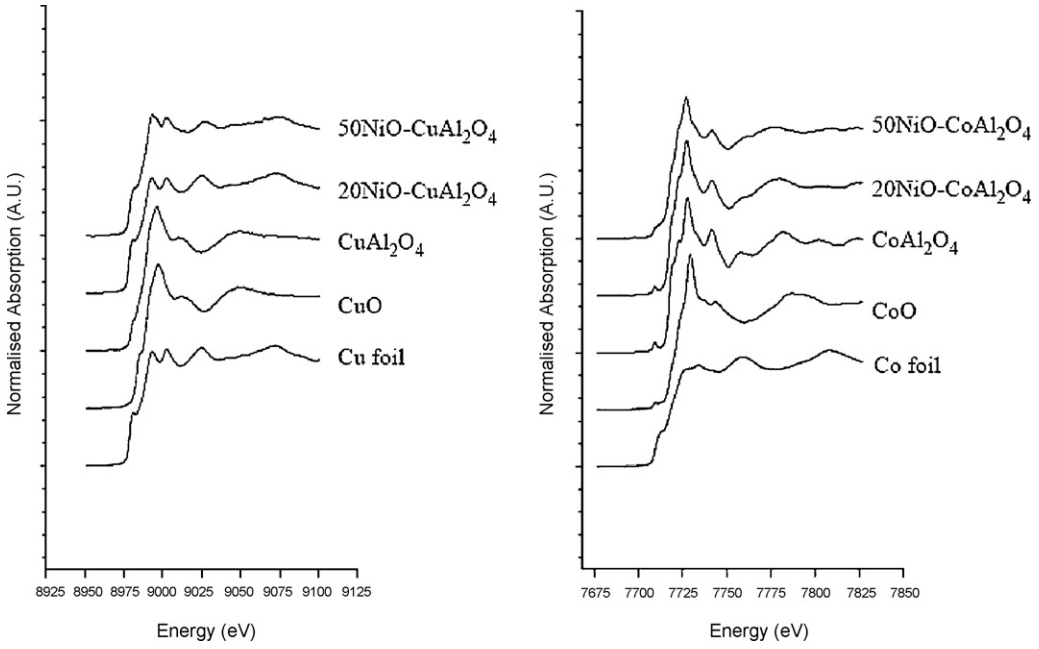

Fig. 7. XANES analyses of the reduced NiO–$CuAl_2O_4$ mixtures and NiO–$CoAl_2O_4$ mixtures as compared to reference compounds.

50 wt% NiO–$CuAl_2O_4$ only has Ni peaks and no Cu peaks. In this case, Cu metal has not disappeared but remains undetected. Lü et al. [26] reported that there are no clear XRD peaks of copper oxide when a small proportion of CuO is mixed with NiO. XANES (Fig. 7 left) data confirm the XRD result that Cu metal exists in Ni–$CuAl_2O_4$ mixture. From these results, it is possible to explain why the Ni–$CuAl_2O_4$ sample shows higher electrical conductivity than any other Ni–**M**Al_2O_4. This is because it has a good metallic phase connection and copper has higher electrical conductivity than nickel (Cu 1.724, Ni 7.24 × 10^{-6} Ω cm at 20 °C [27]).

In the case of Ni–$CoAl_2O_4$, XRD patterns show that the $CoAl_2O_4$ crystal is stable and that Ni peaks overlap with pure $CoAl_2O_4$ patterns (Fig. 5e and f). XANES results also support the hypothesis that Co^{2+} ions in the $CoAl_2O_4$ crystal do not exchange with Ni^{2+} ions when the NiO–$CoAl_2O_4$ mixtures are sintered. It is reported in the literature that $CoAl_2O_4$ crystals have a normal spinel structure with Co^{2+} ions in tetrahedral sites [28]. From XANES results (Fig. 7 right), we observed that the Ni–$CoAl_2O_4$ patterns are very similar to $CoAl_2O_4$ patterns and that Co^{2+} ions in tetrahedral sites form a small pre-edge at 7710 eV [29]. It is thus established that $CoAl_2O_4$ does not change its spinel structure with added NiO and that Co ions remain Co(II) after reduction. Therefore, its microstructure is similar to that of Ni–$NiAl_2O_4$ (Fig. 4), and their electrical properties are almost the same (Fig. 3).

Fig. 8 shows the XRD patterns of Ni–$FeAl_2O_4$ mixtures. After calcining at 1200 °C, hematite (Fe_2O_3) and alumina peaks are detected (Fig. 8a), which indicates to us that $FeAl_2O_4$ crystal has not been synthesized. After calcining at 1400 °C and reducing with hydrogen (Fig. 8b–d), the alumina phase disappears, and magnetite (Fe_3O_4) peaks are detected with intensive peaks of $NiAl_2O_4$ phase. The formation of $NiAl_2O_4$ leads to the consumption of Ni metal, which means that the Ni–$FeAl_2O_4$ mixture has only a small volume of metal-phase Ni (Fig. 4d). This is the reason that its electrical conductivity is very poor.

3.3. Thermal expansion property

The thermal expansion coefficient (TEC) of support material is an essential property in the fabrication of a single cell because thermoelastic mismatch with cell components can cause the bending of support after co-firing or the reduction of mechanical cell strength. Table 1 shows the TEC values of materials that are commercially used in SOFC. In the case of Al_2O_3, its TEC value (8.3 × 10^{-6} K^{-1}) is relatively low compared with that of 8YSZ (10.5 × 10^{-6} K^{-1}). So, the thermal expansion properties of Ni–**M**Al_2O_4 can be adjusted to 8YSZ by controlling Ni content. Our TEC results (Fig. 9), which were measured using a dilatometer, indicate that the reduced NiO–**M**Al_2O_4 mixtures containing 50 wt% NiO have similar TEC values ((9.6–9.9) × 10^{-6} K^{-1}) to that of 8YSZ electrolyte under cell-operating conditions (800–1000 °C). These values can be compared with the TEC of Ni-YSZ mixture (12.6 × 10^{-6} K^{-1}), which is much larger than that of 8YSZ. This degree of appreciable difference between the Ni-YSZ substrate and the electrolyte film might generate stress at the interface and induce degradation of cell performance. Therefore, we used 50 wt% NiO–**M**Al_2O_4 mixtures as single cell supports and measured their cell performances.

Table 1
Thermal expansion coefficients between 25 and 1000 °C of SOFC materials.

Material	(× 10^{-6} K^{-1})
8YSZ	10.5
LSM	11.7
Ni	16.5
Al_2O_3	8.3

3.4. Cell performance

Ni–**M**Al_2O_4-supported single cells were fabricated and operated for comparison with conventional Ni-YSZ cells. Current–voltage curves for the tested single cells are shown in Fig. 10. The peak power density of a Ni-YSZ-supported cell is 490 mW cm^{-2} at 850 °C. Except for Ni–$CuAl_2O_4$, the peak power densities of other Ni–**M**Al_2O_4-based single cells reached about 80% of that of the Ni-YSZ-supported cell. The open circuit voltages (OCV) of Ni–**M**Al_2O_4-supported cells are 1.1 V, which implies both that Ni–**M**Al_2O_4 supports have good co-sintering behavior with YSZ electrolyte and that there is no open-pore in electrolyte layer. Ni–$CuAl_2O_4$-supported samples had little electrochemical performance.

To evaluate the effects of support material on cell performance, the microstructures of the Ni–**M**Al_2O_4-supported cell were examined with SEM–EPMA. Fig. 11 shows the polished cross-sections of Ni–**M**Al_2O_4 substrates after cell operation at 850 °C. In this figure, bright areas indicate YSZ, while light-gray and dark-gray areas indicate Ni metal and **M**Al_2O_4, respectively. Each cell has a dense

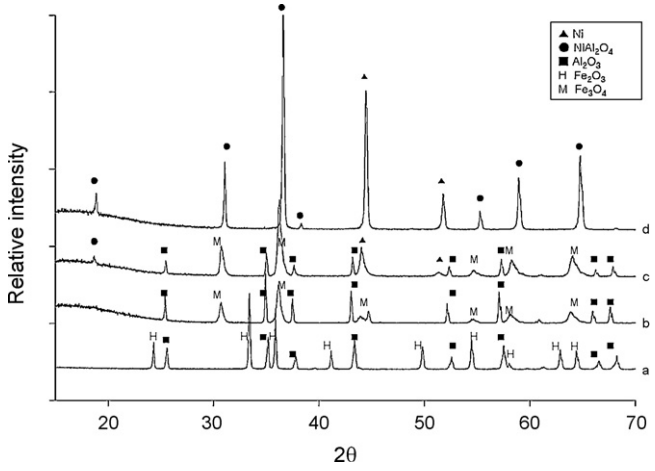

Fig. 8. X-ray diffraction patterns of the Ni–$FeAl_2O_4$ mixtures. (a) 1200 °C calcined $FeAl_2O_4$, (b) reduced $FeAl_2O_4$, (c) reduced $FeAl_2O_4$ with 20 wt% NiO and (d) reduced $FeAl_2O_4$ with 50 wt% NiO.

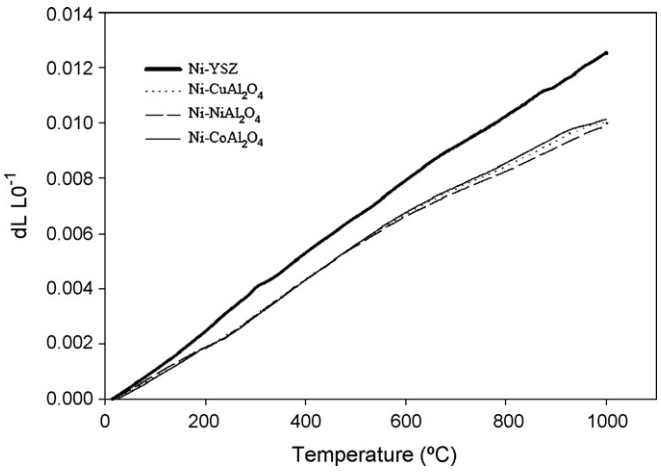

Fig. 9. Thermal expansion curves of Ni-YSZ and Ni–**M**Al_2O_4 mixtures. Each sample containing 50 wt% NiO was sintered at 1400 °C (3 h) and reduced at 850 °C.

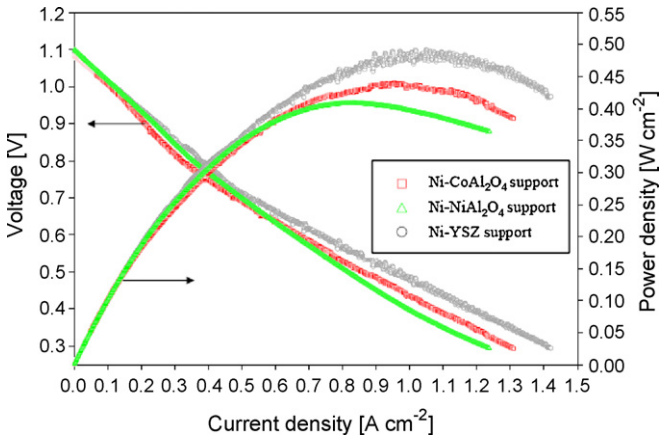

Fig. 10. The current–voltage curves of Ni–**M**Al_2O_4-supported cells at 850 °C, for comparison with conventional SOFC. A Ni-YSZ-supported cell is also shown.

YSZ film (15 μm thickness) and thin Ni-YSZ anode layer that has formed between the electrolyte and the substrate of single cell. In case of Ni–$NiAl_2O_4$- and Ni–$CoAl_2O_4$-supported cells (Fig. 11a and b), each anode layer is composed of the tiny nickel powders with YSZ. In contrast, the anode layer of the Ni–$CuAl_2O_4$-supported cell has no fine particles. YSZ particles of the anode (Fig. 11c) were coarsened to a diameter of 5–10 μm and isolated by the metallic phase. Furthermore, several regions of the anode layer were separated from the electrolyte film. The result of line composition analysis (Fig. 11d) indicates that the metallic phase of the anode layer is composed of Ni and Cu metals. During the co-firing step, copper migrates from the substrate to the anode layer and seems to help the grain growth of Ni-YSZ anode particles due to the fact that the melting point of copper or copper oxide is lower than the co-firing temperature (1400 °C). The formation of this liquid phase accelerates grain growth. The fabrication of a highly porous and finely structured anode is important in order to maximize contact between the gas phase, the electrically conductive electrode, and

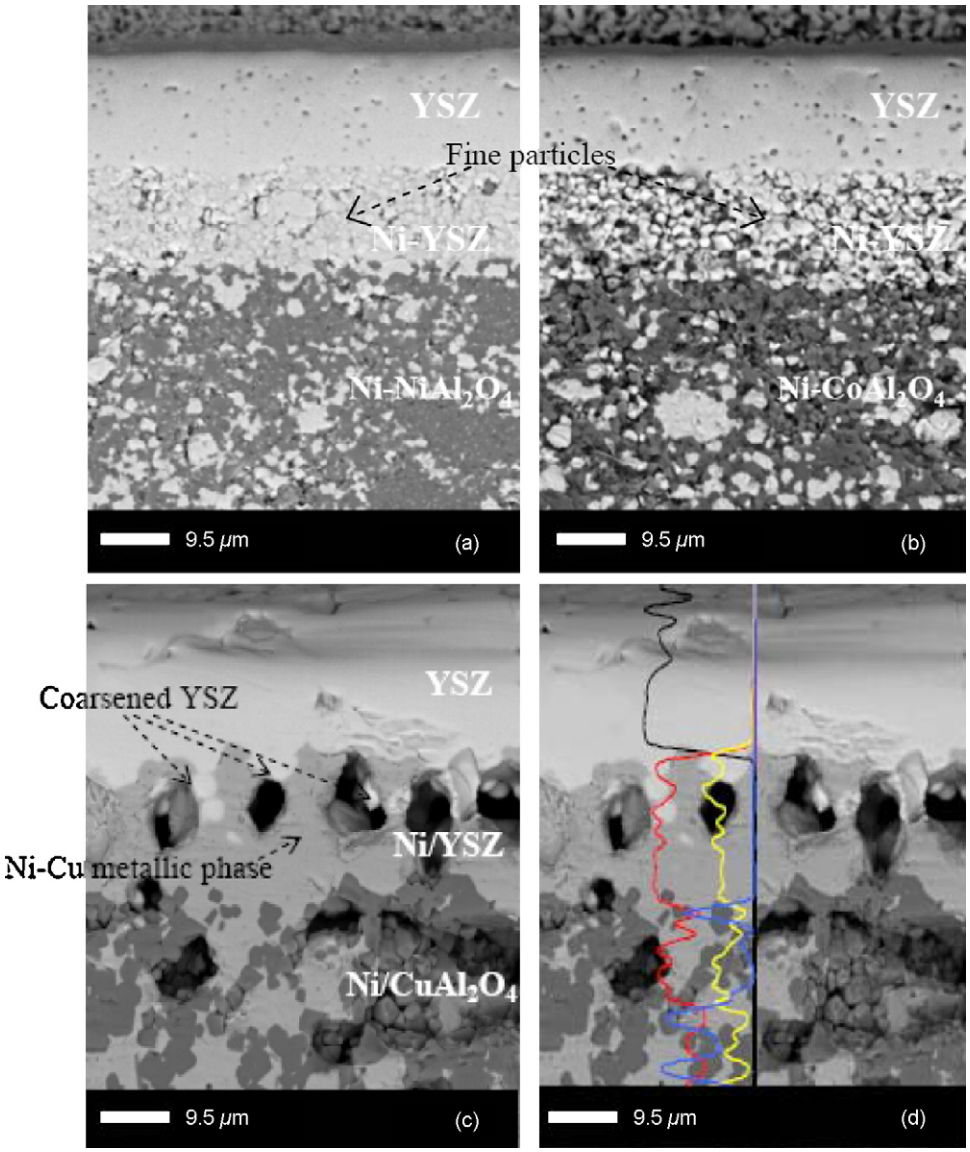

Fig. 11. The cross-sections of (a) Ni–$NiAl_2O_4$-supported cells (b) Ni–$CoAl_2O_4$-supported cells, (c) Ni–$CuAl_2O_4$-supported cells and (d) line composition analysis of Ni–$CuAl_2O_4$-supported cells. Black line: Zr, red line: Ni, yellow line: Cu, blue line: Al. (For interpretation of the references to color in this figure legend, the reader is referred to the web version of the article.)

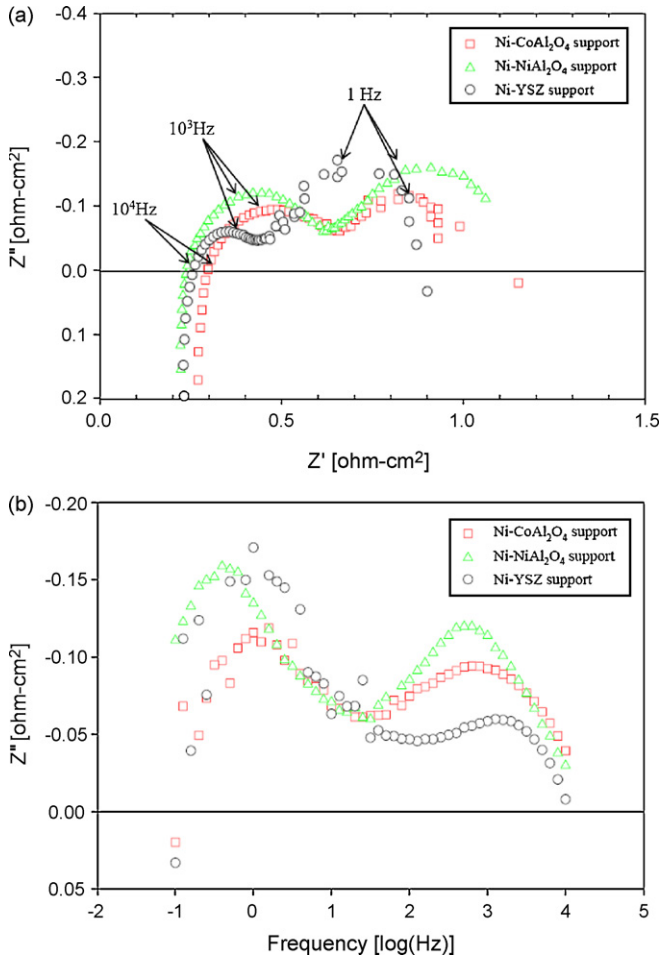

Fig. 12. Impedance spectra of single cells measured at 850 °C in OCV conditions. (a) Cole–Cole plots of Ni–MAl_2O_4-supported cells and (b) the imaginary impedances as functions of AC frequency.

the ion-conductive electrolyte (Triple Phase Boundaries, TPBs). In the case of the Ni–$CuAl_2O_4$-supported cell, however, the agglomeration of anode particles led to a reduction of the amount of TPBs and a detaching of the anode layer from the electrolyte. Therefore, Cu migration and segregation in the anode layer are the reasons why the Ni–$CuAl_2O_4$-supported cell has no electrochemical performance.

The relatively low electrochemical performances of Ni–$\mathbf{M}Al_2O_4$ ($\mathbf{M}$ = Ni, Co)-supported cells result from the difference of polarization resistance. The impedance spectra of the Ni–$\mathbf{M}Al_2O_4$-supported cells are shown in Fig. 12. These results indicate that the ohmic resistance (R_0) of the Ni–$\mathbf{M}Al_2O_4$-supported cell is similar to that of the Ni-YSZ-supported cell. However, the polarization resistances (R_p) of Ni–$\mathbf{M}Al_2O_4$-supported cells are larger than that of the Ni-YSZ-supported cell. The R_ps are increased mainly at the high frequency area (Fig. 12a). Typically, the impedance spectra near the 1000 Hz region are known to be polarization caused by the charge-transfer or surface reaction of the electrode; these polarization resistances are thought to be the main reasons for the degradation of cell performance. When frequencies are less than 10 Hz, the types of cell support do not affect the impedance values (Fig. 12b), and the R_p is related to gas diffusion. That means that Ni–$\mathbf{M}Al_2O_4$ supports have sufficient gas permeability when compared with Ni-YSZ support.

Except for the change of cell support from Ni-YSZ to Ni–$\mathbf{M}Al_2O_4$ mixtures, there is no difference in cell fabrication processes between Ni-YSZ- and Ni–$\mathbf{M}Al_2O_4$-supported cells. Therefore, it can be inferred that the polarization resistances of Ni–$\mathbf{M}Al_2O_4$-supported cells arise in the functional anode layer (FAL). In the case of Ni-YSZ support, the interface contacted with the FAL can participate in anode reaction. However, Ni–$\mathbf{M}Al_2O_4$ supports cannot provide reaction sites because there are no TPBs. It is only the FAL of Ni–$\mathbf{M}Al_2O_4$-supported cells that takes part in the anode reaction. This difference affects the performance of Ni–$\mathbf{M}Al_2O_4$-supported cells, which reduces their peak power densities (Fig. 10). Increased polarization resistances indicate that the FALs of Ni–$\mathbf{M}Al_2O_4$-supported cells lack sufficient catalytic reaction area and that their thickness or microstructure needs to be improved. To increase Ni–$\mathbf{M}Al_2O_4$-supported cell performance, modifications of cell fabrication should also be the subject of further study.

4. Conclusion

Ni–$\mathbf{M}Al_2O_4$ mixtures were fabricated, and their electrical conductivity, microstructure and thermal expansion coefficients were investigated. Among them, Ni–$CuAl_2O_4$ has the highest electrical conductivity because Cu^{2+} ions escape from the metal aluminate structure to generate the Cu metal phase. In the case of the Ni–$FeAl_2O_4$ mixture, Ni forms a $NiAl_2O_4$ crystal, while iron remains in an iron oxide phase, which results in less electrical conductivity (except for the 60 wt% NiO-containing sample). The microstructures of Ni–$NiAl_2O_4$ and Ni–$CoAl_2O_4$ are very similar to each other, and their electrical conductivities are sufficiently high that they can be utilized in SOFC support. The TEC values of Ni–$\mathbf{M}Al_2O_4$ show good affinity with that of 8YSZ. This makes it possible to fabricate Ni–$\mathbf{M}Al_2O_4$-supported single cells that have a 410–440-mW cm^{-2} cell performance at 850 °C. However, the electrochemical performance of SOFC cells using Ni–$\mathbf{M}Al_2O_4$ supports was about 20% lower than that of a conventional Ni-YSZ cell because of the polarization resistance caused by the charge-transfer or surface reaction of anode. This was especially evident for Ni–$CuAl_2O_4$-supported cells, which had no performance due to the Cu migration and segregation problems.

Acknowledgements

The authors would like to thank the financial support from the nanotechnology program of MOST and BK21 program of Korea.

References

[1] J. Palsson, A. Selimovic, L. Sjunnesson, J. Power Sources 86 (2000) 442–448.
[2] Nguyen Q. Minh, Solid State Ionics 174 (2004) 271–277.
[3] Nguyen Q. Minh, J. Am. Ceram. Soc. 76 (1993) 563–588.
[4] A. Atkinson, S. Barnett, R.J. Gorte, J.T.S. Irvine, A. McEvoy, M. Mogensen, S.C. Singhal, J. Vohs, Nature Mater. 3 (2004) 17–27.
[5] S.P.S. Badwal, K. Foger, Ceram. Int. 22 (1996) 257–265.
[6] M. Ippommatsu, H. Sasaki, S. Otoshi, Int. J. Hydrogen Energy 21 (2) (1996) 129–135.
[7] I. Villarreal, C. Jacobson, A. Leming, Y. Matus, S. Visco, L. De Jonghe, Electrochem. Solid-State Lett. 6 (2003) 178–179.
[8] G. Schiller, R. Henne, M. Lang, R. Ruchdäschel, S. Schaper, Fuel Cells Bull. 3 (21) (2000) 7–12.
[9] M. Atsushi, F. Koji, O. Sachio, K. Takeyuki, K. Masafumi, Y. Tetsuo, K. Kenji, I. Minoru, O. Zempachi, Electrochem. Solid-State Lett. 9 (2006) 427–429.
[10] F. Tietz, F.J. Dias, B. Dubiel, H.J. Penkalla, Mater. Sci. Eng. B68 (1999) 35–41.
[11] F. Meschke, F.J. Dias, F. Tietz, J. Mater. Sci. 36 (2001) 5179–5728.
[12] F. Tietz, F.J. Dias, A. Naoumidis, Proceedings of the 3rd European Solid Oxide Fuel Cell Forum, Nantes, 1998, pp. 171–180, vol. 1.
[13] Jeffrey W. Fergus, Solid State Ionics 177 (2006) 1529–1541.
[14] S.H. Clarke, A.L. Dicks, K. Pointon, T.A. Smith, A. Swann, Catal. Today 38 (1997) 411–423.
[15] T. Tatsuya, K. Yukimune, Y. Tatsuya, K. Ryuji, E. Koichi, T. Keigo, U. Yoshitaka, U. Akira, O. Koiji, A. Masanobu, J. Power Sources 112 (2002) 588–595.

[16] S. Park, J.M. Vohs, R.J. Gorte, Nature 404 (2000) 265–267.
[17] N. Kiratzis, P. Holtappels, C.E. Hartwell, M. Morgensen, J.T.S. Irvine, Fuel Cells 1 (2001) 211–218.
[18] S. Primdahl, J.R. Hansen, L. Grahl-Madsen, P.H. Larsen, J. Electrochem. Soc. 148 (1) (2001) A74–A81.
[19] I.S. Metcalfe, R.T. Baker, Catal. Today 27 (1996) 285–288.
[20] A. Al-Ubaid, E.E. Wolf, Appl. Catal. 40 (1988) 73–85.
[21] K.M. Hardiman, C.G. Cooper, A.A. Adesina, Ind. Eng. Chem. Res. 43 (2004) 6006–6013.
[22] J.C. Garland, D.B. Tanner, Electrical Transport and Optical Properties of Inhomogeneous Media, Am. Inst. Phys., New York, 1978.
[23] J.H. Yu, G.W. Park, S. Lee, S.K. Woo, J. Power Sources 163 (2007) 926–932.
[24] D.W. Dees, T.D. Claar, T.E. Easler, D.C. Fee, F.C. Mrazek, Electrochem. Stor. 134 (1987) 2141–2146.
[25] K.-R. Lee, S.H. Choi, J. Kim, H.-W. Lee, J.-H. Lee, J. Power Sources 140 (2005) 226–234.
[26] Z. Lü, L. Pei, T.-M. He, X.-Q. Huang, Z.-G. Liu, Y. Ji, X.-H. Zhao, W.-H. Su, J. Alloy Compd. 334 (2002) 299–303.
[27] CRC Handbook of Chemistry and Physics, 55th edition 1974-1975, CRC Press, F-159.
[28] M. Zayat, D. Levy, Chem. Mater. 12 (2000) 2763–2769.
[29] A.M. Saib, A. Borgna, J. van de Loosdrecht, P.J. van Berge, J.W. Niemantsverdriet, Appl. Catal. A: Gen. 312 (2006) 12–19.